Chemistry, Physics and Technology of Surface. 2022. V. 13. N 4. P. 391-404

UDC 544.723:544.18 doi: 10.15407/hftp13.04.391

E.M. Demianenko [1], M.I. Terets [1], L.M. Ushakova [1], S.V. Zhuravskyi [1], Yu.I. Sementsov [1, 2], V.V. Lobanov [1], O.V. Filonenko [1], V.S. Kuts [1], A.G. Grebenyuk [1], M.T. Kartel [1, 2]

A THEORETICAL STUDY ON THE EFFECT OF HETEROATOMS (N, B, Si) ON THE INTERACTION OF ALUMINUM CLUSTERS WITH A CARBON GRAPHENE-LIKE PLANE

[1] Chuiko Institute of Surface Chemistry of National Academy of Sciences of Ukraine
17 General Naumov Str., Kyiv, 03164, Ukraine, E-mail: demianenko_en@ukr.net
[2] Ningbo University of Technology
201 Fenghua Road, Ningbo, 315211, China

It is known that the addition of a small amount of carbon nanomaterials significantly improves the mechanical properties of composites with a metal matrix. One of the most important, promising and available metals as a matrix for such modification is aluminum. However, at the interface between the carbon material and Al, aluminum carbides of different composition are formed, which are brittle and have the main disadvantage - solubility in water. Therefore, the appearance of aluminum carbide is a serious problem, since it contributes to the formation of defects, which, when the composite is deformed, leads to cracking of the composite due to the presence of microneedles. In this regard, in order to predict the features of the interaction of aluminum itself with the surface of carbon nanomaterials, it is advisable to model such processes using quantum chemistry methods.

The aim of the work was to reveal the effect of temperature on the chemical interaction of aluminum clusters with native, boron-, silicon-, and nitrogen-containing graphene-like planes (GLP).

All the calculated by three methods (B3LYP/6-31G(d,p), MP2/6-31G(d,p) and PBE0/6-31G(d,p)) values of the dependence of the Gibbs free energy on temperature for different cluster sizes of aluminum and graphene-like clusters are the highest for native graphene-like planes. In all cases, the values of the Gibbs free energy increase with temperature.

The lowest values of the temperature dependence of the Gibbs free energy vary as dependent on the size of the reactant models and research methods, this is especially characteristic of the presence of boron and silicon atoms in the graphene-like clusters.

Therefore, the absence of heteroatoms in the composition of the nanocarbon matrix contributes to the fact that aluminum carbide islands should not be formed in the carbon-containing nanocomposite with aluminum, which negatively affects the physical and chemical characteristics of the resulting nanocomposite.

***Keywords**: graphene-like plane, coronene, aluminum nanoclusters, density functional theory method, cluster approximation, aluminum carbide, silicon carbide*

INTRODUCTION

In recent decades, new carbon nanomaterials, in particular nanotubes [1] and graphene [2–3], have attracted much attention due to their unique mechanical and physical properties. In particular, the thickness of graphene is equal to one carbon atom, which makes it the thinnest material known today [4–6]. The theoretical Young's modulus of graphene is 1.0 TPa and its intrinsic tensile strength is 130 GPa, which means that the mechanical properties of graphene are special. In addition, graphene has some other excellent properties, such as high specific surface area, electrical conductivity, and thermal conductivity [7, 8]. Therefore, the study of carbon nanomaterials, in particular, based on graphene as part of metal matrix composites has always been one of the key areas of scientific research [9–13]. Available experimental data show that the addition of a small amount of carbon nanomaterials significantly improves the mechanical properties of composites with a metal matrix [14–16], however, the mechanism of strengthening of carbon nanomaterials in metal composites, and how various factors affect it, has not yet been fully elucidated [17–19].

To study such nanocomposites, in addition to experimental methods, which require a long

period and expensive equipment, computer simulations, in particular methods of molecular dynamics and quantum chemistry, are also successfully used [20–23].

Carbon nanoparticles can be both a strengthening phase and modifiers of the first kind, changing the crystal structure of the matrix metal [24]. However, in addition to the influence of purely geometrical parameters of carbon nanoparticles on the structure of the composite, there is a problem of the formation of the strongest adhesive bonds between the atoms of the metal and the carbon nanoparticle in the composition of the metal composite due to the chemical interaction of the surface carbon atoms of the nanoparticle with the molten metal.

One of the most important, promising and available metal as a matrix for such research work is aluminum. Recently, many publications have been devoted to nanocomposites based on aluminum and carbon materials according to [25–31]. This metal has a low density and its strength approaches or exceeds that of steel. Aluminum also has good ductility, which allows the aluminum alloy to be processed into a variety of profiles. At the same time, excellent corrosion resistance, electrical conductivity and thermal conductivity make aluminum alloy the most widely used non-ferrous structural material in industry. With the development of the aviation, aerospace and automotive industries, higher requirements are constantly put forward for the characteristics of various aspects of materials. Both graphene and aluminum alloy are materials with favorable performance properties, according to the law of mixing, aluminum matrix composites made with graphene as a reinforcing material will perform better than aluminum alloys [32, 33]. Aluminum-graphene composite has a variety of potential applications due to its high strength, low density, and excellent thermal and electrical conductivity [34]. It can be used in the automotive industry, piston combustion chamber to reduce engine emissions at elevated temperatures, transport materials, preparation of defense components, energy carriers, wires and cables in electric vehicle engines, aerospace, space and satellite technologies, *etc*. [35, 36]. This composite can be used to make piston rings, brake pads and various gears. In the aerospace industry, brakes and landing gear can be specially designed. Due to their good electrical conductivity, they can be used to make antennas. Thanks to the increased strength, this composite is suitable to make light bicycles and tennis rackets. These composites have good surface area and high current density potential, making them useful for energy storage. These composites can be used in anodes and coatings [37]. Some literature sources suggest that the addition of graphene increases the electrical properties and microhardness, when incorporated into aluminum to form aluminum-graphene composites, while the literature also reports a deterioration of such properties. They discuss some typical literature reports related to the purpose of this work. Aluminum with 1 wt. % graphene shows an increase in microhardness up to 81 VHN compared to pure Al [38]. The average dispersion of graphene as a reinforcing phase in the matrix is an important factor affecting the characteristics of composite materials [39, 40]. There are strong van der Waals forces between the graphene sheets, which cause agglomeration of graphene in the matrix. The method of mixing directly affects the dispersion of graphene in the matrix. The strength of the interfacial bond between graphene and the aluminum matrix is another important factor that affects the properties of composites [35].

It is well known that aluminum tends to form stable carbide (Al_4C_3) in a wide range of composition [41, 42], therefore aluminum carbide of different composition can form at the interface between carbon material and Al [43, 44]. This substance is fragile and has the main drawback – solubility in water [45]. Therefore, the process of carbide formation is a serious problem, since it contributes to the formation of defects, the presence of which during deformation of the composite leads to the appearance of cracks in the composite due to the presence of Al_4C_3 microneedles, which leads to a sharp decrease in the strength of the composite [46]. However, some authors note that the formation of this carbide will not be as harmful as expected when interacting with multi-walled carbon nanocuts [47], since only the outer layer of CNT reacts, providing an optimal interface with the matrix. However, despite the possibility of effective transfer of the applied load, the use of composite in structures in a humid environment will lead to deterioration of the surface [13]. Therefore, the search for methods

of reducing the formation of aluminum carbide in the nanocomposite is underway [43–49].

In most studies, the authors study the interaction of metal with purely carbon nanoparticles, while there is a large number of modified carbon nanoparticles, the surface chemistry of which is significantly different from that of pure carbon. Such modified carbon nanoparticles can interact with the metal matrix in a different way, and the study of the features of such interaction by theoretical and experimental methods is an urgent task in the modern search for methods of creating new composite materials. One of the methods of such modification can be the doping of the carbon matrix with various heteroatoms, such as N, B, Si, which can significantly change the reactivity of the graphene matrix [50]. It was also found that the influence of such heteroatoms on the interaction of the carbon surface with metals was investigated, using examples of the interaction of carbon fibers with metals in the manufacture of fiber-reinforced metal composites [51]. It was found that the presence of heteroatoms significantly changes the process of interaction between the carbon surface of the filler and the matrix. The surface energy, the wettability of the surface by the molten metal, the reaction rate of the metal and the surface layer of the filler, and the composition of the interphase change. In view of this, it is likely that carbon nanoparticles doped with heteroatoms will have excellent energy characteristics for the formation of aluminum carbide compared to pure carbon materials.

In this regard, in order to predict the specifics of the interaction of aluminum with the surface of carbon nanomaterials supplemented with heteroatoms (N, B, Si), it is advisable to model such processes using theoretical methods.

Therefore, the goal of the work was to find out the effect of temperature on the chemical interaction of aluminum clusters with native, boron-, silicon-, and nitrogen-containing graphene-like planes (GLP) by means of the methods of quantum chemistry.

OBJECTS AND METHODS OF CALCULATION

To study the chemical interaction of a GLP with aluminum, an elementary reaction was considered and respective scheme is shown in Fig. 1, the starting compounds of which are a pure carbon or modified graphene-like plane and an aluminum cluster.

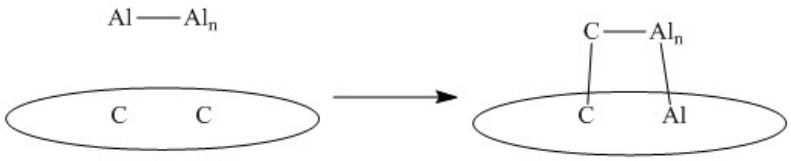

Fig. 1. Diagram of the interaction of a graphene-like plane with aluminum

As a result of the reaction, a chemisorption complex is formed; its feature is the replacement of one of the carbon atoms in the GLP by an aluminum atom, and one of the carbon atoms leaves the plane of the conjugated aromatic system, which indicates the initial stage of the destruction of the GLP with the formation of aluminum carbide [52–54]. Therefore, a number of identical reactions of joining small Al_n clusters to a graphene-like nanocluster (GLN) were considered; they are depicted schematically:

$$Al_n + GLN = Al_nGLN. \quad (1)$$

The energy effects of the reaction (ΔE_{react}) were calculated at a temperature of 0 K without taking into account the energy of zero oscillations (ZPE), according to the scheme (1), due to the following formula (2):

$$\Delta E_{react} = E_{tot}(Al_nGLN) - (E_{tot}(Al_n) + E_{tot}(GLN)), \quad (2)$$

where $E_{tot}(Al_nGLN)$ is the total energy of the interaction product of the metal cluster with GLN, $E_{tot}(Al_n)$ is the total energy of the metal cluster, $E_{tot}(GLN)$ is the total energy of the graphene-like nanocluster.

To take into account the effect of temperature on thermodynamic parameters, the values of the Gibbs free energy of reaction (ΔG_{react}) were calculated in the temperature range from 50 to 1800 K:

$$\Delta G_{react} = G^T(Al_nGLN) - (G^T(Al_n) + G^T(GLN)), \quad (3)$$

where $G^T = E_{tot} + ZPE + G^T_{corr}$, E_{tot} total energy of the corresponding optimized structure, ZPE (zero point vibrational energy) – energy of zero vibrations of the optimized structure, G^T_{corr} – thermodynamic correction of Gibbs free energy [55].

A polyaromatic molecule crowned with $C_{24}H_{12}$ was chosen as the parent GLP (Fig. 2 *a*). Models for modified GLPs were formed by replacing two carbon atoms with nitrogen or boron atoms, forming clusters with the composition $C_{22}N_2H_{12}$ and $C_{22}B_2H_{12}$ (Fig. 2 *b, c*). The $C_{12}Si_{12}H_{12}$ cluster was used as a model of silicon carbide (Fig. 2 *d*).

In addition, to take into account the dimensional effect of the surface of the GLP on thermodynamic parameters, we used a GLP with a gross composition of $C_{42}H_{16}$ (Fig. 2 *e*), as well as nitrogen- ($C_{40}N_2H_{16}$), boron- ($C_{40}B_2H_{16}$), and silicon-containing analogues (Fig. 2 *f–h*).

When examining the interaction of GLPs with aluminum, the latter can be modeled in the cluster approximation, as evidenced by literature data, with small clusters consisting of several atoms [56–58]. Therefore, in our case, aluminum was also modeled by the Al_2 dimer (Fig. 3 *a*) and the Al_4 tetramer, while preliminary calculations (MP2/6-31G(d,p)) for the aluminum dimer indicate that the total energy for the triplet is lower and is -483.726679 Hartree, compared to the ground singlet (-483.691533 Hartree).

Aluminum tetramer can have two isomers – rhombic and tetrahedral (Fig. 3 *b, c*); at the same time, the analysis of calculations using the same method shows that the Al_4 tetrahedral configuration has the lowest energy, as well as for the dimer in the triplet state. Therefore, the cluster (Fig. 3 *c*) with multiplicity 3 was used for simulation of the interaction with GLP.

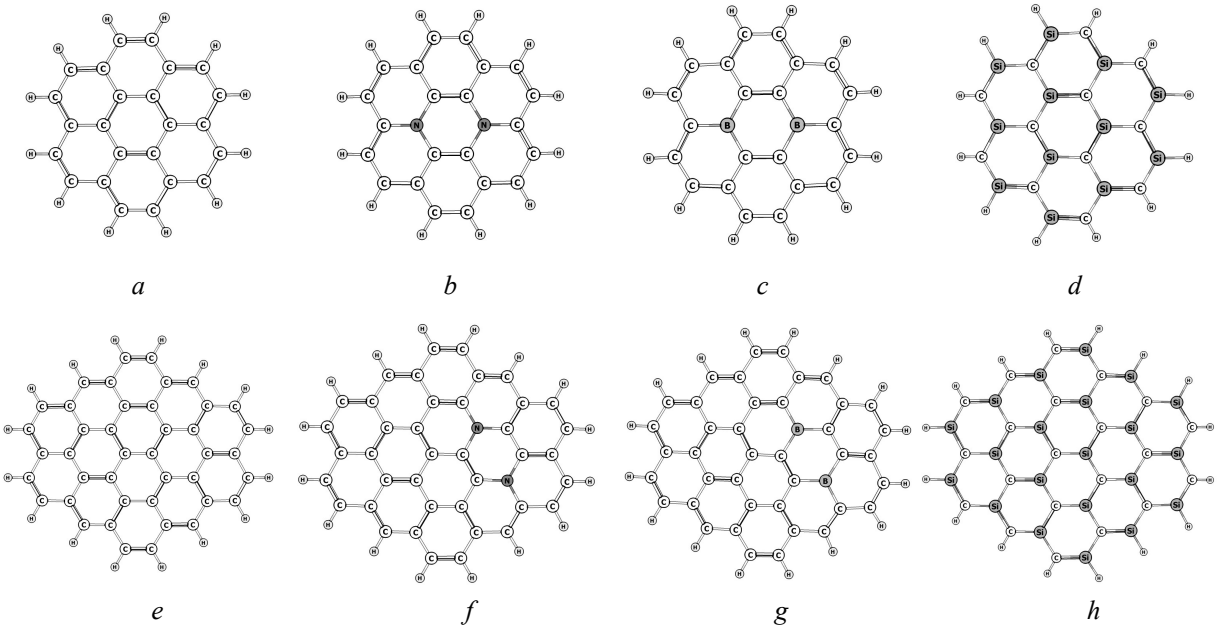

Fig. 2. Equilibrium geometry of the graphene-like plane (*a, e*) and its derivatives: nitrogen-containing (*b, f*), boron-containing (*c, g*), silicon-containing (*d, h*)

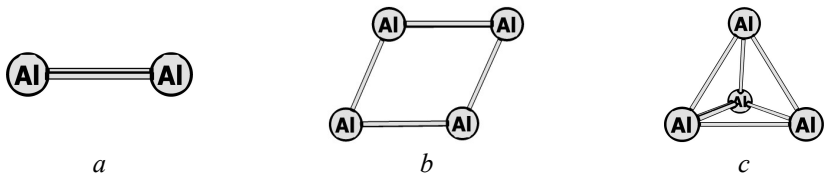

Fig. 3. Equilibrium structure of aluminum dimers (*a*) and tetramers (*b, c*)

Calculations were performed using the GAMESS (US) program [59] within several methods, for greater reliability of simulation results. In particular, by the density functional theory (DFT) method with the B3LYP functional [60, 61], which has proven itself well in modeling graphene-like clusters [62]. We also used the PBE0 functional, which was successfully used for modeling properties and chemical reactions involving clusters of various metals [63–65]. And for comparison, in addition to the DFT method, the second order Moller–Plesset perturbation theory (MP2) [66] was used.

RESULTS AND DISCUSSION

At the beginning, the interaction of the initial GLPs of different sizes with dimers and tetramers of aluminum was considered. In Fig. 4, the optimized by B3LYP/6-31G(d,p) method the interaction products are shown of the aluminum dimer with the coronene molecule ($C_{24}H_{12}$) (Fig. 4 *a*) and with a larger GLP ($C_{42}H_{16}$) (Fig. 4 *b*). When optimized with the PBE0/6-31G(d,p) and MP2/6-31G(d,p) methods, interaction products were obtained with a similar structure to those considered above using the B3LYP/6-31G(d,p) method; therefore, the peculiarities of their structure we do not describe in detail.

As can be seen from this figure, as a result of the interaction of aluminum clusters with the coronene molecule, the plane of the latter is significantly deformed. One of the aluminum atoms is simultaneously bonded to three carbon atoms, and the Al–C bonds are nearly identical and are between 1.87 and 1.88 Å in length. Another aluminum atom has only one Al–C bond with a length of 2.02 Å, which is less than the bond length between two aluminum atoms in the dimer (2.57 Å) (Fig. 4 *a*). The energy effect of reaction (1) calculated by formula (2) is a positive value higher than 200 kJ/mol for all three calculation methods and is +289.2 kJ/mol using the B3LYP/6-31G(d,p) method; a slightly higher value was found using the MP2/6-31G(d,p) method, which is +352.2 kJ/mol; and the lowest value is characteristic of the PBE0/6-31G(d,p) method with a value of +233.8 kJ/ mole (see Table).

When the size of the GLP increases, the structure of the interaction product changes insignificantly, as can be seen from Fig. 4 *b*. The values of energy effects of reactions during their formation are characterized by larger values: for B3LYP/6-31G(d,p) the value increases to +329.2 kJ/mol, for MP2/6-31G(d,p) it is also higher and amounts to +414.5 kJ/mol, and for PBE0/6-31G(d,p) +330.1 kJ/mol, respectively.

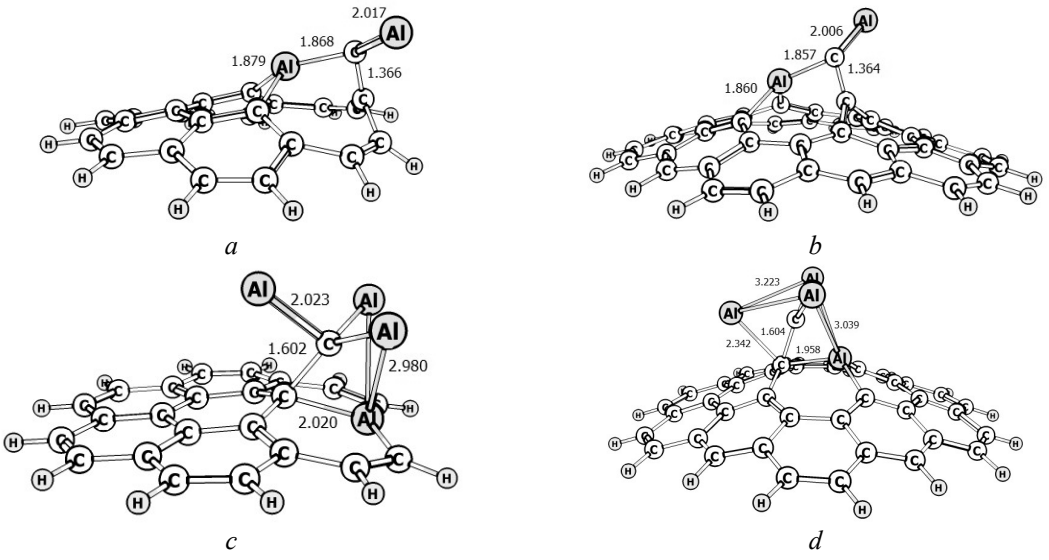

Fig. 4. Equilibrium spatial structure of the interaction products of the dimer (*a, b*) and tetramer (*c, d*) of aluminum with coronene (*a, c*) and the graphene-like $C_{42}H_{16}$ plane (*b, d*)

However, products with aluminum tetramer are similar to each other and have a slightly different structure compared to the product of interaction of GLPs with aluminum dimer (Fig. 4 *c*, *d*). As in the case of the dimer, one of the aluminum atoms placed in the graphene-like

matrix is simultaneously bonded to three carbon atoms in the GLP and two aluminum atoms above the plane. One carbon atom due to substitution by an aluminum atom is concentrated over the aromatic plane and coordinated by three aluminum atoms. Such a difference in structure affects the energetic effect of reaction (1). In particular, for the reaction of aluminum tetrameter with coronene, ΔE_{react}, regardless of the method, is significantly lower than that for similar reactions in the case of aluminum dimer and is only +6.6 kJ/mol for B3LYP/6-31G(d,p), for MP2/6-31G(d,p) it is higher and amounts to +58.7 kJ/mol, and for PBE0/6-31G(d,p) its value is +70.4 kJ/mol, respectively.

In the case of using a larger GLP when interacting with Al_4 (Fig. 4 *d*), the values of the energy effect are similar to the case of the interaction of coronene with Al_2 considered above and have the corresponding values (see Table), namely, for B3LYP/6 -31G(d,p) +252.6, for MP2/6-31G(d,p) it is also higher and is +340.2, and for the PBE0/6-31G(d,p) has a slightly lower value of +214.5 kJ/mol.

The next task was to find out how the above reactions with aluminum are affected by the presence of two nitrogen atoms, which are introduced instead of two carbon atoms in a pair position relative to each other in the central hexagon of the coronene molecule (Fig. 2 *b, f*).

The product of the interaction of an aluminum dimer with a nitrogen-containing analog of coronene (Fig. 5 *a, b*) is structurally similar to the previous one considered above (Fig. 4 *a, b*), in which one of the aluminum atoms is connected to two carbon atoms by bonds with a length of 1.86 Å, as well as with the nitrogen atom of GLP by a bond with a length of 1.81 Å. Between the aluminum atoms, as in the previous case, a carbon atom is placed, and the second aluminum atom is connected to the rest of the molecule by one covalent bond, the length of which is also 1.84 Å (Fig. 5 *a*). However, the Al–C bond is placed perpendicular to the plane of the coronene derivative, unlike the product shown in Fig. 4 *a*. The energetic effects of the reaction of the aluminum dimer and the nitrogen-containing crown-like molecule, regardless of the chosen research method, have negative values, in contrast to those considered in turn. Namely, for B3LYP/6-31G(d,p) the value is -100.4, for MP2/6-31G(d,p) it is higher and is -41.8, and for PBE0/6-31G(d,p) is the lowest and its value is -168.8 kJ/mol (see Table).

When the size of the nitrogen-containing GLP increases, the nature of the bonding of the aluminum dimer with the aromatic part is similar to that discussed above, but the bond lengths increased slightly (Fig. 5 *b*). However, the values of the energy effect acquired a positive value for all three research methods: for B3LYP/6-31G(d,p) +132.0, for MP2/6-31G(d,p) +260.4, and for the PBE0/6-31G(d,p) method it has a slightly lower value of +128.0 kJ/mol.

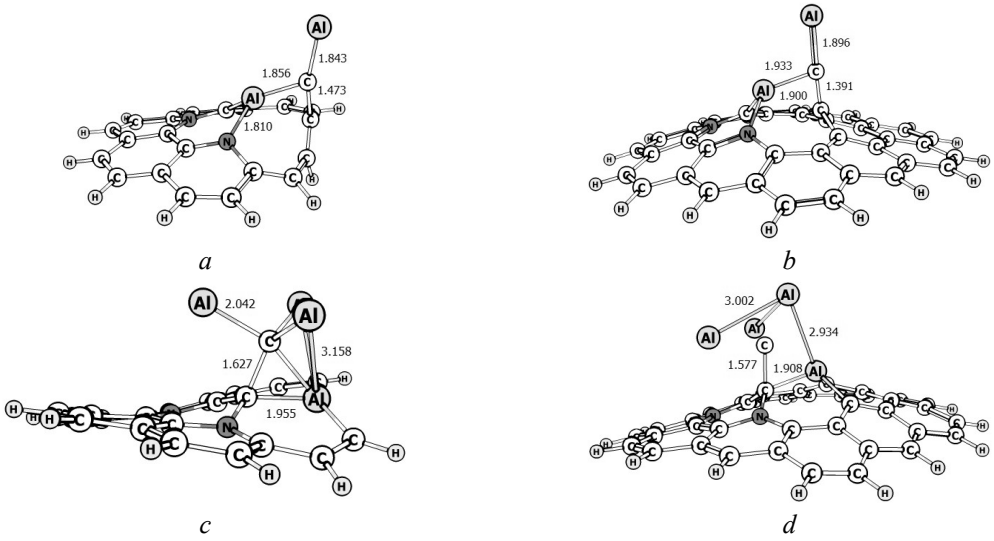

Fig. 5. Equilibrium spatial structure of the interaction products of the dimer (*a, b*) and tetramer (*c, d*) of aluminum and the molecule of the nitrogen-containing derivative coronene (*a, c*) and its enlarged analogue $C_{40}N_2H_{16}$ (*b, d*)

When aluminum tetrameter interacts with nitrogen-containing analogues of coronene and a larger graphene-like plane GLP (Fig. 5 *c, d*), the geometry of the products is similar to those previously considered (Fig. 4 *c, d*). Calculations of the energy effect for nitrogen-containing coronene indicate that this reaction, similar to that with the aluminum dimer, has rather low values; in particular, for B3LYP/6-31G(d,p) it is negative and amounts to -76.8, for MP2/6-31G(d,p) it is slightly positive +6.3, and using the PBE0/6-31G(d,p) method it has a much lower value of -185.4 kJ/mol.

Increasing the size of the nitrogen-containing GLP to ($C_{40}N_2H_{16}$) significantly affects the magnitude of the energy effect (see Table). As in the case of using the same nitrogen-containing GLP, when interacting with an aluminum dimer, the energy effect acquires a positive value of more than 100 kJ/mol when using three different methods; in particular, for B3LYP/6-31G(d,p) it is +149.6, for MP2/6-31G(d,p) ΔE_{react} has an even higher value of +276.6, and the PBE0/6-31G(d,p) method gives the lowest value of +129.0 kJ/mol.

Comparing these values with those for pure GLPs, it should be noted that the presence of nitrogen atoms in the composition of GLPs reduces the energy effect of the interaction with aluminum (see Table).

Next, it was examined how the above reactions with aluminum are affected by the presence of two boron atoms (Fig. 2 *c*), which were placed instead of two nitrogen atoms in the para-position relative to each other in the central hexagon of the coronene derivative.

As can be seen from Fig. 6 *a*, the product of the interaction of an aluminum dimer with a boron-containing coronene derivative significantly differs from the previous nitrogen-containing derivative (Fig. 5 *a*). In particular, aluminum atoms do not form covalent bonds with boron atoms, but only with carbon atoms, the length of which is more than 2 Å. At the same time, the central hexagon of the structure shown in Fig. 1 *c*, as a result of the interaction, turns into a pentagon. However, similar to the previous cases, there is a carbon atom between the aluminum atoms.

The energy effect of the product formation reaction, which is shown in Fig. 6 *a*, has a slightly negative value, for the B3LYP/6-31G(d,p) method it is equal to -2.4 kJ/mol, which is 98.0 kJ/mol less than the similar value for a nitrogen-containing product with aluminum. Calculations by the MP2/6-31G(d,p) method also indicate an increase in the value of ΔE_{react} to +260.8 kJ/mol, however, the analysis of calculations by the PBE0/6-31G(d,p) method shows that in comparison with the atom-containing coronene the energy effect of the reaction with boron increases only slightly from -168.8 to -161.8 kJ/mol.

The use of a larger boron-containing graphene-like surface (Fig. 2 *c*), when interacting with an aluminum dimer, leads to a change in the structure of the reaction product; in particular, the central hexagon of the structure shown in Fig. 6 *a*, does not turn into a pentagon, and Al–C bond lengths are slightly increased for this reaction product. At the same time, the energy effect of the reaction becomes positive regardless of the calculation method: for the B3LYP/6-31G(d,p), the value is +78.6, for MP2/6-31G(d,p) it is higher and is +178.0, and for PBE0/6-31G(d,p) is the lowest and its value is +59.6 kJ/mol, respectively (see Table).

The interaction products of the aluminum tetramer, when interacting with boron-containing analogs of coronene and a larger GLP, have a similar structure to each other (Fig. 6 *c, d*). However, despite this, their energy effects differ significantly. An increase in the size of the boron-containing GLP, regardless of the chosen calculation method, increases the value of the energy effect of the reaction with aluminum tetramer (see Table). In particular, in the case of using the B3LYP/6-31G(d,p) method, the value of ΔE_{react} increases from -231.0 to +53.4 kJ/mol, for the MP2/6-31G(d,p) method - from -72.6 to +170.7 kJ/mol, and for PBE0/6-31G(d,p) the values are traditionally the lowest, and when the size of the GLP increases from $C_{22}B_2H_{12}$ to $C_{40}B_2H_{16}$, the ΔE_{react} values increase from -384.2 to +19.4 kJ /mol

The reaction parameters of silicon-containing coronene with aluminum dimer were also examined. In case of the silicon-containing coronene molecule, unlike previous heteroderivatives, not only two carbon atoms are replaced by silicon ones, but twelve. That is, there is an alternation of carbon and silicon atoms, and their equal number in the molecule allows it to be considered as a model of silicon carbide.

The product of the interaction of a silicon derivative with an aluminum dimer is characterized by the fact that one of the aluminum atoms interacts with two silicon atoms with bond lengths of 2.4 Å (Fig. 7 *a*). Between aluminum atoms, as in all previous cases, there is a carbon atom with Al–C bond lengths of 1.85 and 1.94 Å. In addition, the second aluminum atom is coordinated to the silicon atom at the distance of 2.7 Å.

The energy effect of this reaction has a negative value for the DFT method regardless of the functional and is -25.1 kJ/mol for the B3LYP and -128.1 kJ/mol for PBE0 respectively. Calculation by the MP2/6-31G(d,p) method shows a positive value of the energy effect of this reaction, namely +65.4 kJ/mol.

When using an enlarged substrate (Fig. 2 *h*), the geometry of the product became slightly different from the previous one (Fig. 7 *b*). In particular, as can be seen from this figure, one of the aluminum atoms is not bonded to any other except the carbon atom with a bond length of 1.905 Å. Calculations of the energy effect of this reaction by three different methods differ significantly from each other. For the MP2/6-31G(d,p) method it is +78.1, and for PBE0/6-31G(d,p) it is negative and its value is -43.7, and for the B3LYP method /6-31G(d,p) value is the highest and (+233.2 kJ/mol).

The products of the interaction of the aluminum tetramer with the silicon-containing derivative coronene (Fig. 7 *c*) and its enlarged analogue (Fig. 7 *d*) are visually similar to each other. In them, aluminum atoms are bonded to both carbon and silicon atoms. It should be noted that the values of ΔE_{react} for these two interaction products, regardless of the calculation methods, are negative and when the size of the GLP increases, these values become more positive. In particular, the B3LYP/6-31G(d,p) method shows that the value of ΔE_{react} increases from -158.1 to -134.7 kJ/mol, for the MP2/6-31G(d,p) method - from -81.0 to -22.2 kJ/mol, and for PBE0/6-31G(d,p), as in the previous cases, they are the lowest, and when the size of the GLP increases from $C_{12}Si_{12}H_{12}$ to $C_{21}Si_{21}H_{16}$, the values of the energy effect of this reaction increase from -280.0 to -190.3 kJ/mol.

As evidenced by the results of the calculation of the Gibbs free energy of the interaction of aluminum dimers with a coronene derivative (Fig. 8 *a, b, c*) and its enlarged analogue (Fig. 8, *d, e, f*), calculated according to formula (3), in the temperature range from 50 to 1800 K, in all considered cases this value increases.

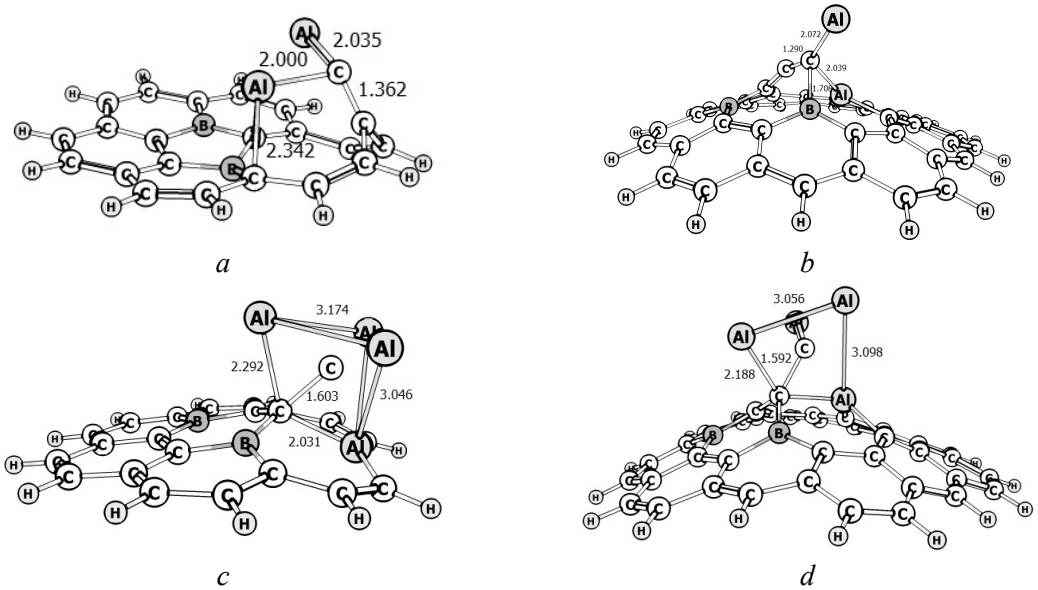

Fig. 6. Equilibrium spatial structure of the interaction products of dimer (*a, b*) and tetramer (*c, d*) of aluminum from a molecule with boron-containing coronene ($C_{22}B_2H_{12}$) (a, c) and boron-containing graphene-like plane ($C_{40}B_2H_{16}$) (*b, d*)

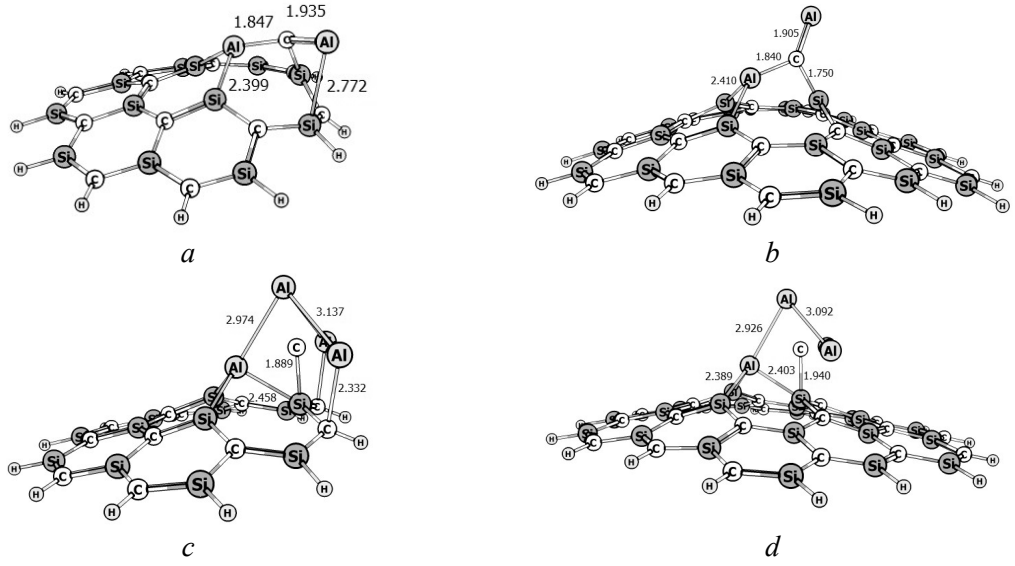

a *b* *c* *d*

Fig. 7. Equilibrium spatial structure of the interaction products of the dimer (*a, b*) and tetramer (*c, d*) of aluminum from the silicon-containing derivative coronene (*a, c*) and the enlarged analogue $C_{21}Si_{21}H_{16}$ (*b, d*)

Table. Energy effects (ΔE_{react}) of the reaction of the interaction of dimers and tetramers of aluminum with graphene-like planes (in kJ/mol)

Reactive compounds	Calculation methods		
	MP2	**B3LYP**	**PBE0**
$Al_2+C_{24}H_{12}$	+352.2	+289.2	+233.8
$Al_2+C_{22}N_2H_{12}$	-41.8	-100.4	-168.8
$Al_2+C_{22}B_2H_{12}$	+260.8	-2.4	-161.8
$Al_2+C_{12}Si_{12}H_{12}$	+65.4	-25.1	-128.1
$Al_2+C_{42}H_{16}$	+414.5	+329.2	+330.1
$Al_2+C_{40}N_2H_{16}$	+260.4	+132.0	+128.0
$Al_2+C_{22}B_2H_{16}$	+178.0	+78.6	+59.6
$Al_2+C_{21}Si_{21}H_{16}$	+78.1	+233.2	-43.7
$Al_4+C_{24}H_{12}$	+58.7	+6.6	+70.4
$Al_4+C_{22}N_2H_{12}$	+6.3	-76.8	-185.4
$Al_4+C_{22}B_2H_{12}$	-72.6	-231.0	-384.2
$Al_4+C_{12}Si_{12}H_{12}$	-81.0	-158.1	-280.0
$Al_4+C_{42}H_{16}$	+340.2	+252.6	+214.5
$Al_4+C_{40}N_2H_{16}$	+276.6	+149.6	+129.0
$Al_4+C_{22}B_2H_{16}$	+170.7	+53.4	+19.4
$Al_4+C_{21}Si_{21}H_{16}$	-22.2	-134.7	-190.3

At the same time, as can be seen from Fig. 8, regardless of the research method and the size of the GLP, the largest value of the Gibbs free energy of the aluminum dimer interaction is available for a pure GLP and it increases with increasing temperature. The position of the $\Delta G_{react}(T)$ curve depends on the research method and the size of the graphene-like cluster. In particular, for the horse-shaped plane, the B3LYP/6-31G(d,p) and MP2/6-31G(d,p) methods show that the lowest $\Delta G_{react}(T)$ curve is characteristic of the nitrogen-containing plane, and the PBE0/6-31G(d,p) method, generally shows that the lowest $\Delta G_{react}(T)$ curve is

characteristic of a boron-containing GLP. When the size of the graphene-like cluster increases, a different picture is observed, namely, the MP2/6-31G(d,p) and PBE0/6-31G(d,p) methods indicate that the lowest curve is characteristic of the silicon-containing plane (Fig. 8 *e, f*). The B3LYP/6-31G(d,p) method shows that the curve for the boron-containing graphene-like cluster is the lowest (Fig. 8 *d*).

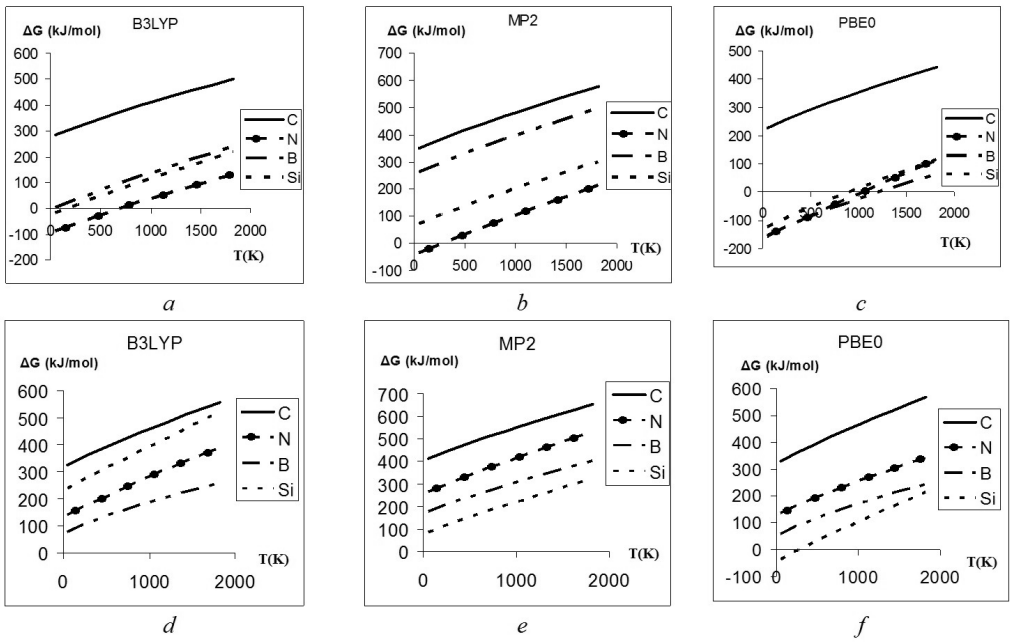

Fig. 8. Temperature dependence of the Gibbs energy of the interaction of aluminum dimers with the coronene derivative (*a, b, c*) and its enlarged analogue (*d, e, f*)

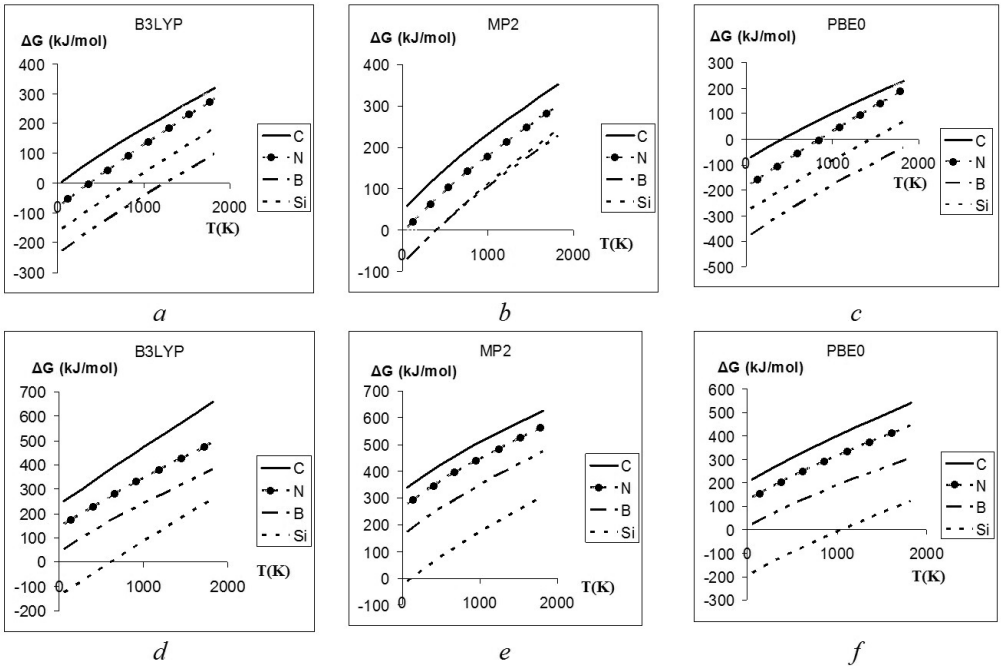

Fig. 9. Temperature dependence of the Gibbs energy of the interaction of aluminum tetramers with a coronene derivative (*a, b, c*) and its enlarged analogue (*d, e, f*)

For a similar reaction when using an aluminum tetramer, similarly to the previous case, the plot of the $\Delta G_{react}(T)$, regardless of the research method and the size of the graphene-like cluster, which belongs to the interaction of the aluminum tetrameter and a pure GLP without heteroatoms present in it, is the highest placed (Fig. 9). In addition, as can be seen from this figure, all values of the dependence of the Gibbs free energy, as in the previous case, also increase with increasing temperature.

For a cluster of a smaller size, all three methods show that the curve with the crown-like plane containing the crown is the lowest (Fig. 9 *a, b, c*). When the aluminum tetramer interacts with a larger GLP, regardless of the calculation method, it shows that the lowest placed curve belongs to the silicon-containing GLP.

CONCLUSIONS

All plots of the Gibbs free energy on temperature, regardless of the size of aluminum clusters and the size of graphene-like clusters, calculated by three methods (B3LYP/6-31G(d,p), MP2/6-31G(d,p) and PBE0/6-31G(d,p)) are the highest for native graphene-like planes. In all cases, these values increase with increasing temperature.

The lowest plots of the Gibbs free energy on temperature vary as dependent on the size of the reactant models and research methods, however, the most cases are characterized by the presence of boron and silicon atoms in the graphene-like clusters.

Therefore, the absence of heteroatoms in the composition of the nanocarbon matrix best contributes to the fact that aluminum carbide islands will not form in the carbon-containing nanocomposite with aluminum, which negatively affects the physical and chemical characteristics of the obtained nanocomposite.

Теоретичне дослідження впливу гетероатомів (N, B, Si) на взаємодію кластерів алюмінію з вуглецевою графеноподібною площиною

Є.М. Дем'яненко, М.І. Терець, Л.М. Ушакова, С.В. Журавський, Ю.І. Семенцов, В.В. Лобанов, О.В. Філоненко, В.С. Куць, А.Г. Гребенюк, М.Т. Картель

Інститут хімії поверхні ім. О.О. Чуйка Національної академії наук України
вул. Генерала Наумова, 17, Київ, 03164, Україна, demianenko_en@ukr.net
Ніньбо технологічний університет
вул. Феньхуа 201, Ніньбо, 315211, Китай

Відомо, що додавання невеликої кількості вуглецевих наноматеріалів значно покращує механічні властивості композитів з металевою матрицею. Одним із найбільш важливим, перспективним та доступним металом як матриці для подібної модифікації є алюміній. Однак на межі поділу між вуглецевим матеріалом та Al утворюється карбіди алюмінію різного складу, які є крихкими і мають головний недолік – розчинність у воді. Тому поява карбіду алюмінію є серйозною проблемою, оскільки це сприяє утворенню дефектів, які при деформації композиту приводять до розтріскування композиту внаслідок наявності мікроголок. У зв'язку з цим, для передбачення особливостей взаємодії саме алюмінію з поверхнею доповнених гетероатомами (N, B, Si) вуглецевих наноматеріалів, доцільно провести моделювання таких процесів методами квантової хімії. Метою роботи було з'ясувати вплив температури на хімічну взаємодію кластерів алюмінію з нативною, бор-, силіций- та нітрогенвмісними графеноподібними площинами (ГПП). Всі розраховані трьома методами (B3LYP/6-31G(d,p), MP2/6-31G(d,p) та PBE0/6-31G(d,p)) значення залежності вільної енергії Гібса від температури як для різних розмірів кластерів алюмінію, так і графеноподібних кластерів, є найвищими для нативних графеноподібних площин. У усіх випадках, значення вільної енергії Гібса зростають з температурою. Найнижчі значення температурної залежності вільної енергії Гібса змінюються від розміру моделей реагуючих речовин і методів дослідження, особливо це характерно за наявності в складі графеноподібних кластерів атомів бору та кремнію. Отже, відсутність домішкових гетероатомів у складі нановуглецевої матриці сприяє тому, що у вуглецьвмісному нанокомпозиті з алюмінієм не будуть утворюватись острівці карбіду алюмінію, який негативно впливає на фізичні та хімічні характеристики одержаного нанокомпозиту.

***Ключові слова**: графеноподібна площина, коронен, нанокластери, метод теорії функціонала густини, кластерне наближення, карбід алюмінію, карбід кремнію*

REFERENCES

1. De Volder M.F.L., Tawfick S.H., Baughman R.H., Hart A.J. Carbon nanotubes: present and future commercial applications. *Science.* 2013. **339**(6119): 535.
2. Geim A.K., Novoselov K.S. The rise of graphene. *Nat. Mater.* 2007. **6**: 183.
3. Sahu D., Sutar H., Senapati P., Murmu R., Roy D. Graphene, Graphene-Derivatives and Composites: Fundamentals, Synthesis Approaches to Applications. *J. Compos. Sci.* 2021. **5**(7): 181.
4. Li Z., Fu X., Guo Q., Zhao L., Fan G., Li Z., Xiong D.B., Su Y., Zhang D. Graphene quality dominated interface deformation behavior of graphene-metal composite: The defective is better. *Int. J. Plast*. 2018. **111**: 253.
5. Hu Z., Tong G., Lin D., Chen C., Guo H., Xu J., Zhou L. Graphene-reinforced metal matrix nanocomposites – a review. *Mater. Sci. Technol*. 2016. **32**: 930.
6. Muxi L., Yuhong Z., Liwen C., Jianquan L., Ting Z., Hua H. Research progress on preparation technology of graphene-reinforced aluminum matrix composites. *Mater. Res. Express*. 2019. **6**(3): 032002.
7. Lee C, Wei X.D., Kysar J.W., Hone J. Measurement of the Elastic Properties and Intrinsic Strength of Monolayer Graphene. *Science*. 2008. **321**(5887): 385.
8. Williams J.C., Starke E.A.Jr. Progress in structural materials for aerospace systems. *Acta Mater*. 2003. **51**(19): 5775.
9. Bakshi S.R., Lahiri D., Agarwal A. Carbon nanotube reinforced metal matrix composites - a review. *Int. Mater. Rev*. 2010. **55**(1): 41.
10. Silvestre N. State-of-the-art Review on Carbon Nanotube Reinforced Metal Matrix Composites. *Int. J.Compos. Mater.* 2013. **3**(6A): 28.
11. Ghodrati H., Ghomashchi R. Effect of graphene dispersion and interfacial bonding on the mechanical properties of metal matrix composites: An overview. *FlatChem.* 2019. **16**: 100113.
12. Doğan K., Özgün M.İ., Sübütay H., Salur E., Eker Y., Kuntoğlu M., Aslan A., Gupta M.K., Acarer M. Dispersion mechanism-induced variations in microstructural and mechanical behavior of CNT-reinforced aluminum nanocomposites. *Archiv. Civ. Mech. Eng.* 2022. **22**: 55.
13. Chen W., Yang T., Dong L., Elmasry A., Song J., Deng N., Elmarakbi A., Liu T., Lv H.B., Fu Y.Q. Advances in graphene reinforced metal matrix nanocomposites: Mechanisms, processing, modelling, properties and applications. *Nanotech. Precis. Eng.* 2020. **3**(4): 189.
14. Ameri S., Sadeghian Z., Kazeminezhad I. Effect of CNT addition approach on the microstructure and properties of NiAl- CNT nanocomposites produced by mechanical alloying and spark plasma sintering. *Intermetallics*. 2016. **76**: 41.
15. Huang Z., Zheng Z., Zhao S., Luo P., Chen L. Copper matrix composites reinforced by aligned carbon nanotubes: mechanical and tribological properties. *Mater. Des*. 2017. **133**: 570.
16. Bor A., Ichinkhorloo B., Uyanga B., Lee J., Choi H. Cu/CNT nanocomposite fabrication with different raw material properties using a planetary ball milling process. *Powder Technol*. 2018. **323**: 563.
17. Zhang X., Zhao N., He C. The superior mechanical and physical properties of nanocarbon reinforced bulk composites achieved by architecture design – a review. *Prog. Mater. Sci.* 2020. **113**: 100672.
18. Zhao Z., Bai P., Du W., Liu B., Pan D., Das R., Liu C., Guo Z. An overview of graphene and its derivatives reinforced metal matrix composites: preparation, properties and applications. *Carbon.* 2020. **170**: 302.
19. Montazeri A., Mobarghei A. Nanotribological behavior analysis of graphene/metal nanocomposites via MD simulations: new concepts and underlying mechanisms. *J. Phys. Chem. Solids.* 2018. **115**: 49.
20. Xing C., Sheng J., Wang L., Fei W. Research progress in molecular dynamics simulation of CNT and graphene reinforced metal matrix composites. *Oxford Open Mater. Sci.* 2021. **1**(1): itab008.
21. Kumar S., Pattanayek S.K., Das S.K. Reactivity-Controlled Aggregation of Graphene Nanoflakes in Aluminum Matrix: Atomistic Molecular Dynamics Simulation. *J. Phys. Chem. C.* 2019. **123**(29): 18017.
22. Nasiri S., Wang K., Yang M., Guénolé J., Li Q., Zaiser M. *Atomistic aspects of load transfer and fracture in CNT-reinforced aluminium.* (Materialia, Elsevier, 2022).
23. Faria B., Guarda C., Silvestre N., Lopes J.N.C. Aluminum composites reinforced by γ-graphynes: The effect of nanofillers porosity and shape on crystal growth and composite strengthening. *Comput. Mater. Sci.* 2020. **176**: 109538.
24. Zhou X., Liu X., Lei J., Yang Q. Atomic simulations of the formation of twist grain boundary and mechanical properties of graphene/aluminum nanolaminated composites. *Comput. Mater. Sci*. 2020. **172**: 109342.
25. Zhang S., Chen G., Qu T., Wei J., Yan Y., Liu Q., Zhou M., Zhang G., Zhou Z., Gao H., Yao D., Zhang Y., Shi Q., Zhang H. A novel aluminum-carbon nanotubes nanocomposite with doubled strength and preserved electrical conductivity. *Nano Res.* 2021. **14**: 2776.

26. Zhang L., Hou G., Zhai W., Ai Q., Feng J., Zhang L., Si P., Ci L. Aluminum/graphene composites with enhanced heat-dissipation properties by in-situ reduction of graphene oxide on aluminum particles. *J. Alloys Compd.* 2018. **748**: 854.
27. Jia H., Fan J., Liu Y., Zhao Y., Nie J., Wei S. Study on fabrication and properties of Graphite/Al composites by hot isostatic pressing-rolling process. *Materials*. 2021. **14**(10): 2522.
28. Shao P., Sun K., Zhu P., Liu K., Zhang Q., Yang W., Wang, Z., Sun M., Zhang D., Kidalov S., Xiao H., Wu G. Enhancing the strengthening effect of graphene-nanoplates in Al matrix composites by heterogeneous matrix design. *Nanomater*. 2022. **12**(11): 1833.
29. Lou S.M., Qu C.D., Guo G.X., Ran L.W., Liu Y.Q., Zhang P.P., Su C.J., Wang Q.B. Effect of fabrication parameters on the performance of 0.5 wt. % graphene nanoplates-reinforced aluminum composites. *Mater.* 2020. **13**(16): 3483.
30. Faria B., Guarda C., Silvestre N., Lopes J.N.C. Aluminum composites reinforced by γ-graphynes: The effect of nanofillers porosity and shape on crystal growth and composite strengthening. *Comput. Mater. Sci*. 2020. **176**: 109538.
31. Mohammed S.M.A.K., Chen D.L. Carbon nanotube-reinforced aluminum matrix composites. *Adv. Eng. Mater.* 2020. **22**(4): 1901176.
32. Starke E.A.Jr., Staley J.T. Application of modern aluminum alloys to aircraft. *Prog. Aerosp. Sci.* 1996. **32**(2–3): 131.
33. Shia Z.J., Wang Z.B., Wang X.D., Zhang S., Zhen Y.G. Effect of thermally induced B2 phase on the corrosion behavior of an $Al_{0.3}$CoCrFeNi high entropy alloy. *J. Alloys Compd*. 2022. **903**: 163886.
34. Palei B.B., Dash T., Biswal S.K. Graphene reinforced aluminum nanocomposites: synthesis, characterization and properties. *J. Mater. Sci.* 2022. **57**(18): 1.
35. Palei B.B., Dash T., Biswal S.K. A review on recent advances of aluminium/graphene nanocomposite. *PalArch's J. Archaeol. Egypt/Egyptol*. 2020. **17**(7): 10119.
36. Pourmand N.S., Asgharzadeh H. Aluminum matrix composites reinforced with graphene: a review on production, microstructure, and properties. *Crit. Rev. Solid State Mater. Sci.* 2019. **45**(4): 289.
37. Bakshi S.R., Lahiri D., Agarwal A. Carbon nanotube reinforced metal matrix composites - a review. *Int. Mater. Rev.* 2010. **55**(1): 41.
38. Sun C., Song M., Wang Z., He Y. Effect of particle size on the microstructures and mechanical properties of SiC reinforced pure aluminum composite. *J. Mater. Eng. Perform*. 2011. **20**: 1606.
39. Tjong S.C. Recent progress in the development and properties of novel metal matrix nanocomposites reinforced with carbon nanotubes and graphene nanosheets. *Mater. Sci. Eng. R. Rep.* 2013. **74**(10): 281.
40. Xu C., Wang X., Zhu J.W. Graphene−metal particle nanocomposites. *J. Phys. Chem. C.* 2008. **112**(50): 19841.
41. Kuzumaki T., Miyazawa K., Ichinose H., Ito K. Processing of carbon nanotube reinforced aluminum composite. *J. Mater. Res*. 1998. **13**(9): 2445.
42. Okamoto H. Phase Diagram updates: section III: Al-C (Aluminum-Carbon). *J. Phase Equilibria.* 1992. **13**: 97.
43. Xu D.K., Rometsch P.A., Birbilis N. Improved solution treatment for an as-rolled Al–Zn–Mg–Cu alloy. Part I. Characterisation of constituent particles and overheating. *Mater. Sci. Eng. A*. 2012. **534**: 234.
44. Xu C.L., Wei B.Q., Ma R.Z., Liang J., Ma X.K., Wu D.H. Fabrication of aluminum–carbon nanotube composites and their electrical properties. *Carbon.* 1999. **37**(5): 855.
45. Kuzumaki T., Miyazawa K., Ichinose H., Ito K. Processing of carbon nanotube reinforced aluminum composite *J. Mater. Res.* 1998. **13**(9): 2445.
46. Ahmad S.I., Hamoudi H., Abdala A., Ghouri Z.K., Youssef K.M. Graphene-reinforced bulk metal matrix composites: synthesis, microstructure, and properties. *Rev. Adv. Mater. Sci.* 2020. **59**(1): 67.
47. Esawi A.M.K, Morsi K., Sayed A., Gawad A.A., Borah P. Fabrication and properties of dispersed carbon nanotube–aluminum composites. *Mater. Sci. Eng. A.* 2009. **508**(1–2): 167.
48. Zhao W., Zhao Z., Bai P., Zhang L., Han B., Du W. The Interfacial Characteristics of graphene/Al_4C_3 in Graphene/$AlSi_{10}Mg$ composites prepared by selective laser melting: first principles and experimental results. *Material*s. 2020. **13**(3): 702.
49. Ali A.M., Omar M.Z., Hashim H., Salleh M.S., Fadhlina I. Mohamed Recent development in graphene-reinforced aluminium matrix composite: A review. *Rev. Adv. Mater. Sci.* 2021. **60**(1): 801.
50. Strelko V.V., Kuts V.S., Thrower P.A. On the mechanism of possible influence of heteroatoms of nitrogen, boron and phosphorus in a carbon matrix on the catalytic activity of carbons in electron transfer reactions. *Carbon*. 2000. **38**(10): 499.
51. Chang K., Gu D. Direct metal laser sintering synthesis of carbon nanotube reinforced Ti matrix composites: Densification, distribution characteristics and properties. *J. Mater. Res*. 2016 **31**(2): 281.

52. Chen X., Qian F., Bai X., Zhao D., Zhang X., Li J., He C., Shi C., Tao J., Zhao N. Formation of the orientation relationship-dependent interfacial carbide in Al matrix composite affected by architectured carbon nanotube. *Acta Mater.* 2022. **228**: 117758.
53. Sadeghi B., Cavaliere P., Pruncu C.I. Architecture dependent strengthening mechanisms in graphene/Al heterogeneous lamellar composites. *Mater. Character.* 2022. **188**: 111913.
54. Qiu Z., Zhang Z., Xiong Y., Luo X., Li Z., Zheng K., Hu W. Size effects of graphene sheets on the strengthening mechanism of Al-graphene composites: A molecular dynamics study. *Appl. Surf. Sci.* 2022. **596**: 153546.
55. Demianenko E., Ilchenko M., Grebenyuk A., Lobanov V. A theoretical study on orthosilicic acid dissociation in water clusters. *Chem. Phys. Lett*. 2011. **515**(4–6): 274.
56. Matveev A.V., Neyman K.M., Pacchioni G., Rosch N. Density functional study of M_4 clusters (M=Cu, Ag, Ni, Pd) deposited on the regular MgO(001) surface. *Chem.Phys. Lett*. 1999. **299**(6): 603.
57. Ma L., Wang J., Hao Y., Wang G. Density functional theory study of $FePd_n$ (n = 2–14) clusters and interactions with small molecules. *Comput. Mater. Sci.* 2013. **68**: 166.
58. Montejo-Alvaro F., Oliva J., Herrera-Trejo, M. Hdz-García H. M., Mtz-Enriquez A.I. DFT study of small gas molecules adsorbed on undoped and N-, Si-, B-, and Al-doped graphene quantum dots. *Theor. Chem. Acc.* 2019. **138**: 37.
59. Barca G., Bertoni C., Carrington L., Datta D., De Silva N., Deustua J.E., Fedorov D.G., Gour J.R., Gunina A.O., Guidez E., Harville T., Irle S., Ivanic J., Kowalski K., Leang S.S., Li H., Li W., Lutz J.J., Magoulas I., Mato J., Mironov V. Recent developments in the general atomic and molecular electronic structure system. *J. Chem. Phys.* 2020. **152**(15): 154102.
60. Becke A.D. Density functional thermochemistry. III. The role of exact exchange. *J. Chem. Phys*. 1993. **98**(7): 5648.
61. Lee C., Yang W., Parr R.G. Development of the Colle-Salvetti correlation-energy formula into a functional of the electron density. *Phys. Rev. B.* 1988. **37**(2): 785.
62. Voitko K., Tóth A., Demianenko E., Dobos G., Berke B., Bakalinska O., Grebenyuk A., Tombácz E., Kuts V., Tarasenko Y., Kartel M., László K. Catalytic performance of carbon nanotubes in H_2O_2 decomposition: Experimental and quantum chemical study. *J. Colloid Interf. Sci.* 2015. **437**: 283.
63. Ernzerhof M., Scuseria G.E. Assessment of the Perdew−Burke−Ernzerhof exchange-correlation functional. *J. Chem. Phys.* 1999. **110**(11): 5029.
64. Dimakis N., Gupta S., Wadud R., Bhatti M.I. Computational data of molybdenum disulfide/graphene bilayer heterojunction under strain. *Data in Brief.* 2022. **42**: 108054.
65. Jabed M.A., Zhao J., Kilin D., Yu T. Understanding of light absorption properties of the N-doped graphene oxide quantum dot with TD-DFT. *J. Phys. Chem. C.* 2021. **125**(27): 14979.
66. Head-Gordon M., Pople J.A., Frisch M.J. MP2 energy evaluation by direct methods. *Chem. Phys. Lett.* 1988. **153**(6): 503.

Received 12.04.2022, accepted 05.12.2022